RESEARCH ARTICLE

Cytotoxicity and photocatalytic activity of Tl doped CeO_2 nanoparticles

Ali Alizadeh[1*]

[1]*Department of Digital Health, School of Medicine, Tehran University of Medical Sciences, Tehran, Iran*

ARTICLE INFO

Article History:
Received 09 Oct 2022
Accepted 15 Nov 2022
Published 15 Feb 2023

Keywords:
Tl-CeO₂-NPs
Prosopis fracta
photocatalytic
MDA-MB-231

ABSTRACT

This paper presents an easy way for the preparation of pure and thallium doped cerium oxide nanoparticles (Tl-CeO_2-NP) through of *Prosopis fracta*. The physicochemical properties of the obtained NP were determined through the PXRD, FESEM/PSA/EDX, UV-Vis/DRS, and Raman analyzing techniques. The FESEM images showed their porous morphology, as well as their altered particle size as a result of being doped of metal. The photocatalytic activity of NP on Methylene blue (MB) dye was tested and observed the higher degradation performance of Tl-CeO_2-NP. The toxicity effect of pure and Tl-CeO_2-NP on breast cancer cell (MDA-MB-231) line survey by application of MTT test. There were no signs of any cytotoxic on MDA-MB-231 cells throughout finding of NP. In this regard, the performance of a doping process led to the production of non-toxic NP that proved to be applicable for drug delivery purposes and even industrial applications such as dye photodegradation and removal of pollutions.

How to cite this article
Alizadeh A., Cytotoxicity and photocatalytic activity of Tl doped CeO2 nanoparticles. Nanomed Res J, 2023; 8(1): 61-68.
DOI: 10.22034/nmrj.2023.01.006

INTRODUCTION

In recent years, significant efforts were made on the development of nanoparticles/nanocrystals towards new applications in certain areas including cosmetics, environmental protection, medicine, and biology [1]. Nanoparticles have the ability to adjust the properties of materials through various parameters such as shapes, morphologies, and surface-to-volume ratios[2, 3].

Cerium (Ce) belongs to a rare earth class and cerium dioxide (CeO_2) is considered the stable type of cerium oxide [4]. Next to being the second most reactive element in the lanthanide series, cerium is electrically positive in the dual oxidation states of Ce^{+3} and Ce^{+4}. It usually contains two types of oxides known as cerium dioxide (CeO_2) and cesium trioxide (Ce_2O_3), while commonly CeO_2 is used as cerium oxide due to its higher stability than Ce_2O_3. Considering the importance of oxygen vacancy in cerium oxide, they can be exerted in various industrial, medical, and biological fields, such as solar cells, catalysts, cancer treatment, pollutant removal, and photocatalytic applications, which also gradually attracted the attention of nanotechnology researchers by their unique features [5, 6].

Breast cancer is the second most common cancer among women with an increased rate of three to four times in recent decades [7]. Nanotechnology can help in designing and providing tools to target cancer cells and enhance their effectiveness. In fact, the focus of worldwide relative research activities is to pave the way for the medical application of nanotechnology to provide a timely identification and radical fight against cancer. Nanotechnology can help to bring about fundamental changes in the treatment and caring approaches of cancer. Nanoparticles play a unique and vital role in the conversion of knowledge into clinically useful advancements in order to revolutionize the process of diagnosis and treatment of cancer cells and ultimately lead to its prevention [8, 9]. As an example, recent studies on cerium oxide nanoparticles were indicative of their cytotoxic on cancer cells and so, assessments are necessary to specify the side effects of its application in the treatment of cancer [10-12].

* Corresponding Author Email: *alizadeh@tums.ac.ir*

Today, the occurrence of environmental pollution by the dyes of textile industry effluents has become one of the most important environmental outcomes [13]. Color is the most obvious characteristic of textile industry effluents. The types of dyes are categorized into anionic (acidic and reactive dyes), cationic (base dyes), and non-ionic. Azo dyes are accountable for 60 to 70% and reactive dyes make up 20 to 25% of the exerted dyes in industry. Due to the lack of proper fixation of dye molecules on the fibers and the inefficiency of dyeing units, unfortunately, 20% of these dyes enter the industrial effluent due to the improper fixation of molecules on the fibers and the incompetence of dyeing units. In addition, dyes were proved to be carcinogenic and mutagenic to humans. Therefore, it is crucial and inevitable to discover a suitable treatment method in accordance with the existing standards [13, 14].

Considering the superior importance of removing dyes from wastewater than colorless organic matter, various methods were investigated and reported for the dispatching of paint from water and sewage. These approaches include biological processes, combinations of biochemical and chemical processes, chemical oxidation, adsorption, coagulation, and fungal processes, while each method implicate its own advantages and disadvantages. The low efficiency of conventional biological treatment systems in dye removal is caused by the high toxicity of dyes towards microorganisms and their resistance to biodegradation. Ultrasound and reverse osmosis techniques are not economically viable through their high operating costs, while other common procedures are also limited for the same reason. Since none of the available methods are capable of performing an effective removal, it is very important to attempt and discover an alternative solution to this problem [15]. Advanced oxidation procedures based on photocatalytic reactions have attracted the interest of many in the past several years due to their effectiveness in mineralizing pollutants and avoiding the obstacle of residues. Photocatalytic approach is one of the advanced oxidation processes with the ability to remove a variety of toxic and degradable compounds. Metal nanoparticles and metal oxides are the main and most widely used nanostructured catalysts. The reaction of nanometer catalyst particles is more significant than larger particles or bulk materials due to their surface-to-volume ratio. According to many studies, cerium oxide nanoparticles can be considered as an ideal, cost-effective, and environmentally friendly photocatalyst [16, 17].

Therefore, this study attempted to synthesize pure and doped cerium oxide nanoparticles by thallium through a simple and fast route by using *Prosopis fracta* in order to evaluate their functionality and cytotoxic activity on breast cancer (MDA-MB-231) cell lines. We investigated the photocatalytic nature of our NP on the degradation of MB dye.

MATERIALS AND METHOD

Prepare of pure and Tl-CeO_2-NPs

To start the prepare of CeO_2 NPs, 20 mL of *Prosopis fracta* extract was initially prepared to be mixed with $Ce(NO_3)_2.6H_2O$ (0.1 M, Merck) solution and stirred for 2 h at 70 ˚C. In the following, the resulted solution was dried at 80 ºC for 20 h to be calcinated for 1:30 hours at 400 ˚C and result in the achievement of yellow CeO_2 nanopowders.

The synthesis of Tl-CeO_2-NPs required the preparation of 20 mL of *Prosopis fracta* extract in Erlenmeyer's to be mixed with $Ce(NO_3)_2.6H_2O$ (0.01 M, Merck) solution. According to the formula of $X_{1-x}Ce_xO_2$ (x=5% W/W), tillum nitrate were weighted and then added to Elran. Obtained solution stirred for 2 h at 70 ˚C, they dried at 80 ˚C for 20 h and then calcinated for 1:30 hours at 400 ˚C.

NP Characterization

The prepared pure and doped CeO_2 NPs were characterized by various analyzing technics. The crystalline nature of synthesized nanoparticles was studied by PXRD analysis (Netherlands, PANalyticalX'Pert PRO MPD system, Cu Kα), while their absorption spectroscopy was identified by UV-Vis (Halo DB-20 UV-Vis double beam). The vibrational modes of the samples were captured by Raman spectra (Raman Takram P50C0R10, laser wavelength of 532 nm), and their surface morphology and particle size distribution were determined by FESEM (MIRA3 TESCAN, Czech) analysis.

Cytotoxic assay

MTT Test

Human breast cancer (MDA-MB-231) cells were cultured with a high glucose DMEM that was supplemented with 10% fetal bovine serum

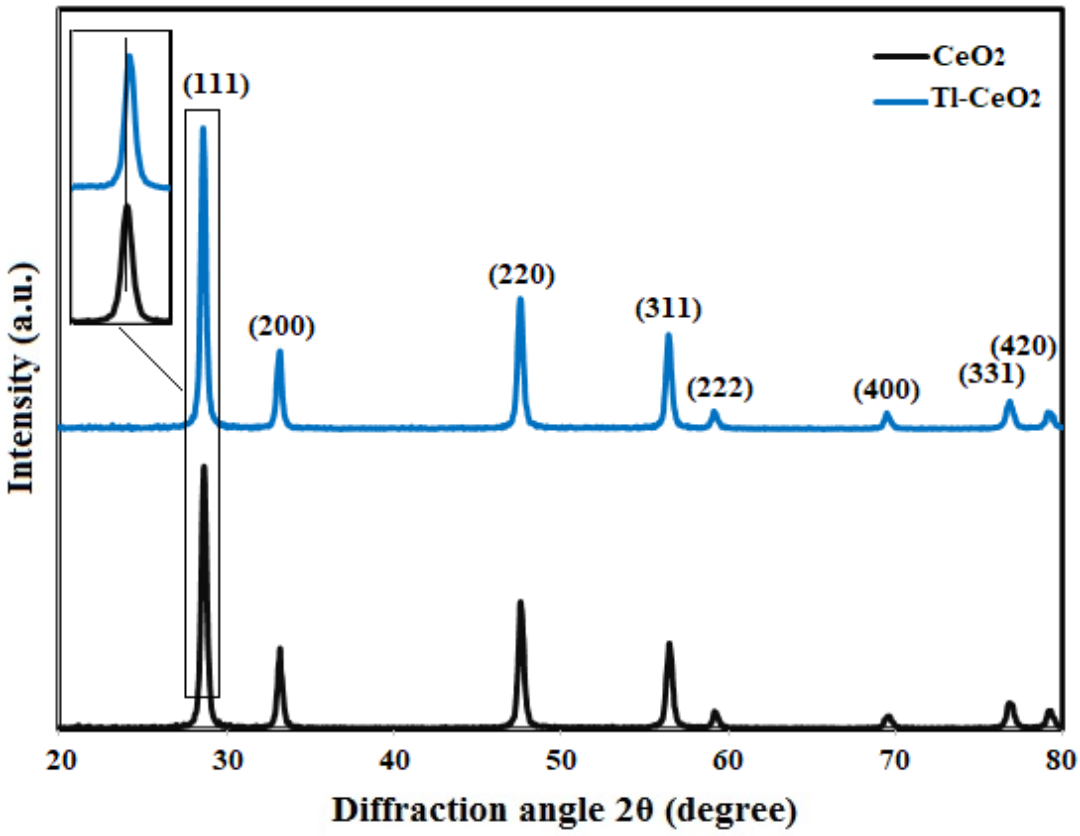

Fig. 1. XRD diagram of pure and Tl-CeO2-NP by Prosopis fracta extract

and 1% penicillin/streptomycin solution in an incubator (37 ˚C, 5% CO_2), which was continued until the cell count of each well reached 10000. The culture medium was replaced with 100 µL of DMEM that contained the formulations at different concentrations (0-1000 µg/mL) to be seeded for another 24 hours. Each concentration had three duplications. Once the culture medium was changed after 24 hours to be replaced with fresh high glucose DMEM, 20 µL of 5 mg/mL 3-(4, 5-dimethylthiazol-2-yl)-2, 5-diphenyl tetrazolium bromide (MTT) solution was added to each well to be further incubated for 4 hours. Subsequent to adding 100 µL of DMSO to each well, the resulting mixture was shaken for about 15 minutes at room temperature to dissolve the formazan. The optical density (OD) was measured at 570 nm by the usage of a microplate reader and the rate of cell viability (VR) was calculated through the following equation:

$$VR = A/A_0 \times 100\% \quad (1)$$

Where A is the absorbance of cells that were treated with formulations and A_0 refers to the absorbance of control group. The results were reported based on the mean ± standard deviation by the usage of SPSS 15 statistical software. The student t-test was exerted for the statistical analysis ($p \leq 0.05$).

Photocatalytic test

The photocatalytic activity of pure and Tl-CeO_2-NP was investigated in UVA-11W light under the conditions of primary dye standard solution, pH=11, dye concentration of 10^{-5} M, and 3 mg of nanoparticles (10^{-3} M). The sampling was done for 270 minutes, while the absorption rate was read at 30 minutes time intervals by the application of a spectrophotometer. The percentage of photocatalytic degradation was calculated through equation 2.

$$\text{Dye degradation}(\%) = (A_0 - A_t)/A_0 \times 100 \quad (2)$$

In which A_0 stands for the primary absorption of methylene blue and A_t is the absorption of solution at t time.

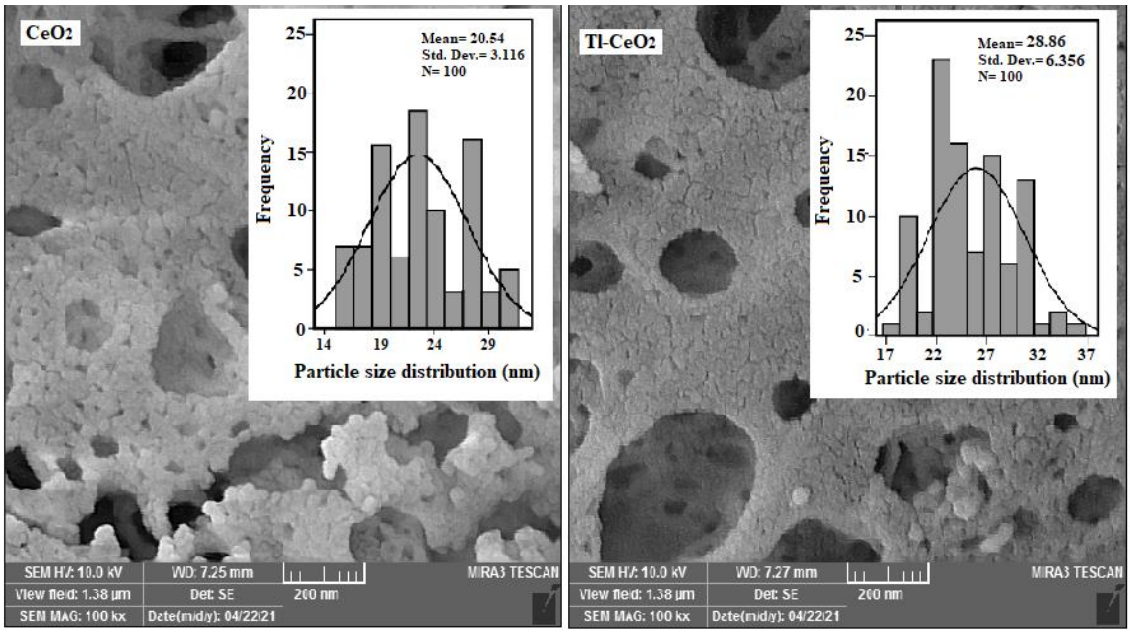

Fig. 2. FESEM images and PSA curve of pure and Tl-CeO2-NPs by Prosopis fracta extract

RESULTS & DISCUSSION

PXRD

The PXRD graph of pure and Tl-CeO_2-NP is depicted in Fig. 1. The graph of pure CeO_2 NP displayed several peaks that were in correspondence with (111) (200) (220) (311) (222) (400) (331) and (420) levels of cerium oxide (ICDD PDF No. 00-043-1002) with the space group of Fm3m, which indicated the purity and cubic fluorite structure of these nanoparticles [10]. According to Fig. 1, the observance of a slight change in (111) peak referred to the entry of Tl doped into the crystalline structure of CeO_2 NP. The crystalline size of pure and Tl-CeO_2-NP were estimated through the Scherer equation [18][20] to be 26.12, and 32.87 nm, respectively. The crystalline size of doped nanoparticles is bigger than that of the pure NP. This increase was apparently caused by the higher ionic radius of Tl^{+1} (1.64 Å) than the ionic radius of cerium (1.03 Å).

FESEM/PSA/EDAX

Fig. 2 presents the SEM images of pure and Tl-CeO_2-NP. As it is observed, the synthesized NP contain porous structure and since their particle size was changed by the doping of Tl, the recorded particles in the FESEM image of Tl-CeO_2-NP were larger in size. Similar to the data of PXRD section, this observation was due to the larger ion radius of thallium when compared to cerium. In conformity to Fig. 2, the presented particle size distribution of synthesized NP in PSA curve was obtained to be 20.54 and 28.86 nm for pure and Tl-CeO_2-NPs, respectively. These results are quiet in agreement with the PXRD outcomes. The quantitative elemental analysis was performed through the EDAX technique and the obtained EDAX spectra of pure, Tl-CeO_2-NPs are exhibited in Fig. 3. These spectra display the cerium and thallium absorptions very clearly, which confirms the presence of every doped element in its doped nanoparticle spectrum.

Raman

The Raman spectra of pure and Tl-CeO_2-NP are depicted in Fig. 4. Accordingly, the fcc crystalline structure of pure CeO_2-NP was once again approved by the detected Raman active band F2g at 457 cm^{-1} in the graph of pure CeO_2-NP, which may be associated with the fluorite structure. In addition, the doping of different metals into the structure of CeO_2 caused an alteration in the intensity band of 457 cm^{-1}. D.A. Gómez *et al* stated that the intensity of Raman signals can be dependent on the particle size[19]. As it was mentioned in the XRD and FESEM sections, the doping of bismuth, lead, and thallium metals changed the size of doped CeO_2-NP as a result of their different ionic radius. Considering the size of doped nanoparticles, the peak intensity of Tl-CeO_2-NP was observed to be higher than other nanoparticles, which is caused by their larger particle size.

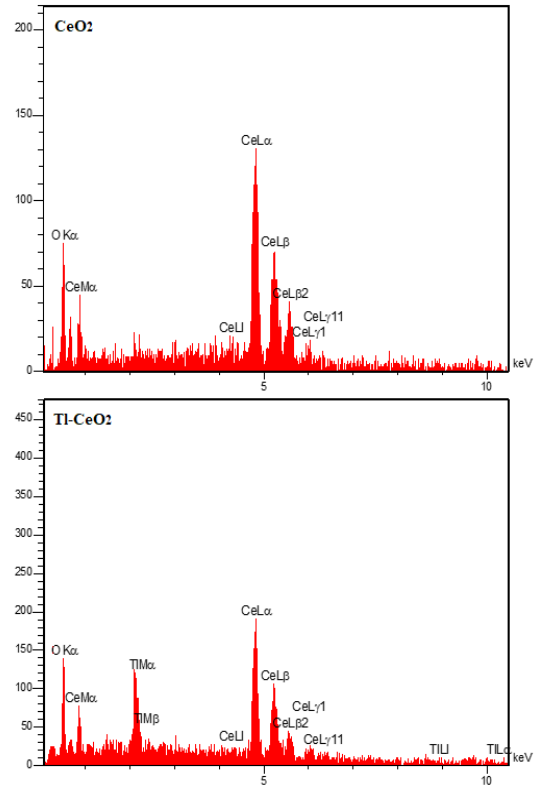

Fig. 3. EDAX images of pure and Tl-CeO2-NP by Prosopis fracta extract

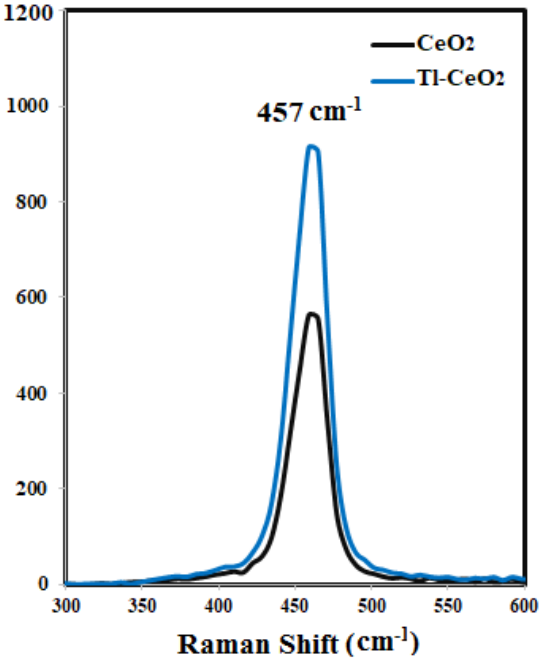

Fig. 4. Raman spectra of pure and Tl-CeO2-NP by Prosopis fracta extract

UV-Vis and DRS

Fig. 5 displays the UV-visible absorption spectra of pure and Tl-CeO_2-NP, which is primarily used to achieved the band gap of materials and also record the induced alterations in the energy band structure of CeO_2 upon the doping of Tl metal. In conformity to Fig. 5(A), the optical absorption depicted some absorption peaks at the regions of 340 and 347 nm that were related to pure and Tl-CeO_2-NP, respectively. Considering the mentioned particle size of doped NP in the XRD and FESEM sections, increasing the rate of doped metals with their larger radical ions than that of cerium caused a red shift in the position of absorption spectra towards the higher wavelengths [20].

The DRS spectra of pure and Tl-CeO_2-NP are exhibited in Fig. 5(B). Considering the absorption data, the energy gap (Eg) of obtained nanoparticles was determined through the following equation:

$$(\alpha h\nu)^2 = A(h\nu - Eg) \quad (2)$$

Where α refers to the absorption coefficient, hν is the photon energy, and A stands for a constant that would be independent of photon energy. According to Fig. 5(B), the band gap of CeO_2-NP was observed to be 3.53 eV, which was decreased as the particle size of doped nanoparticles was increased and resulted in the values of 3.47 eV for Tl-CeO_2-NP, respectively. These values are higher than that of the bulk CeO_2 (Eg ~ 3.19 eV) [20]. Quantum confinement effect can be the reason behind the detected decrease in the band gap and inducement of red shift.

Cytotoxic activity

Today, nanoscience was highly developed in various medical fields, including the treatment of cancer, since the various types of this disease have become very common and caused the suffering of many people. The available treatments, such as chemotherapy, radiotherapy, etc., along with the therapeutic dimension resulted in causing unpleasant complications for the patients. Therefore, scientists and researchers seek to develop therapeutic approaches to combat this deadly disease. Meanwhile, next to the great expansion of nanoscience and nanotechnology, their various fields, including nanoparticles, are widely exerted for a variety of medical applications [1].

This work attempted to investigate the cytotoxic activity of synthesized pure and Tl-CeO_2-NP against breast cancer cells (MDA-MB-231). The experimental cells were exposed to different

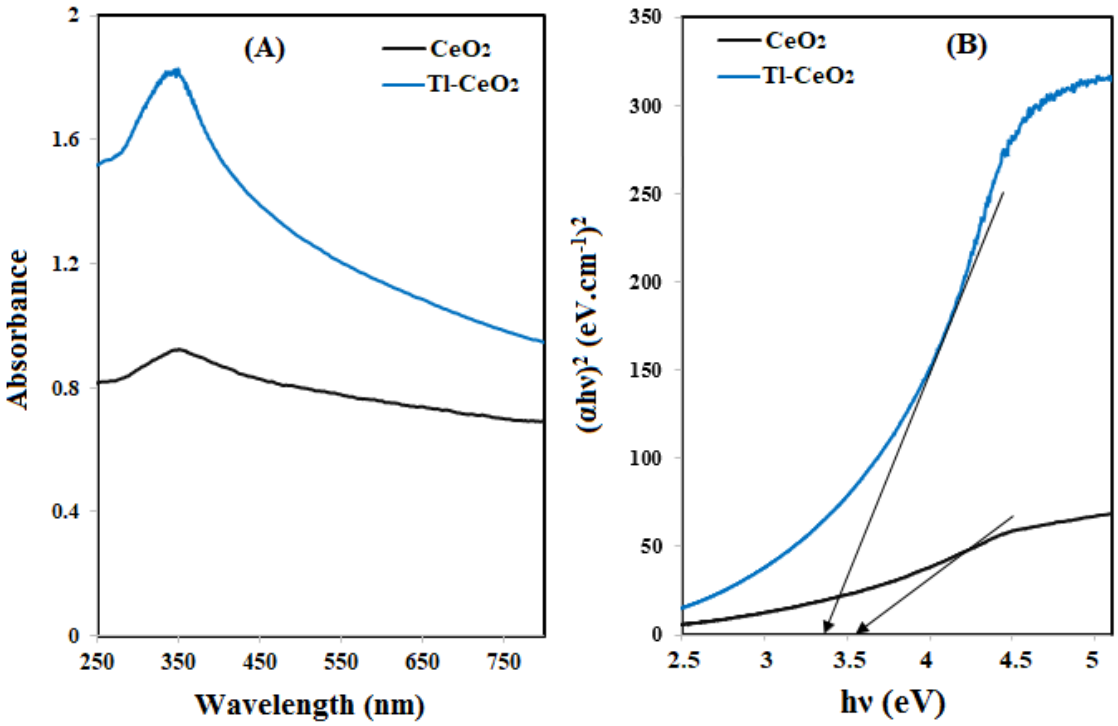

Fig. 5. (A) UV-Vis absorption spectra and (B) DRS of pure and Tl-CeO2-NP by Prosopis fracta extract

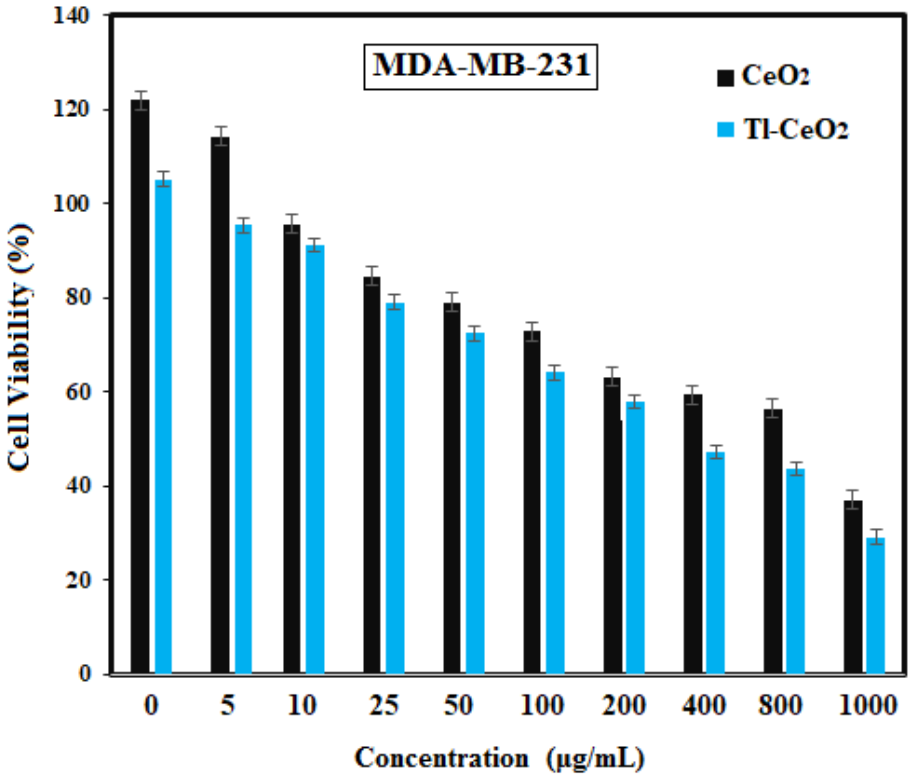

Fig. 6. Cytotoxic effect of pure and Tl-CeO2-NP on breast cancer (MDA-MB-231) cells after 24 hours treatment time.

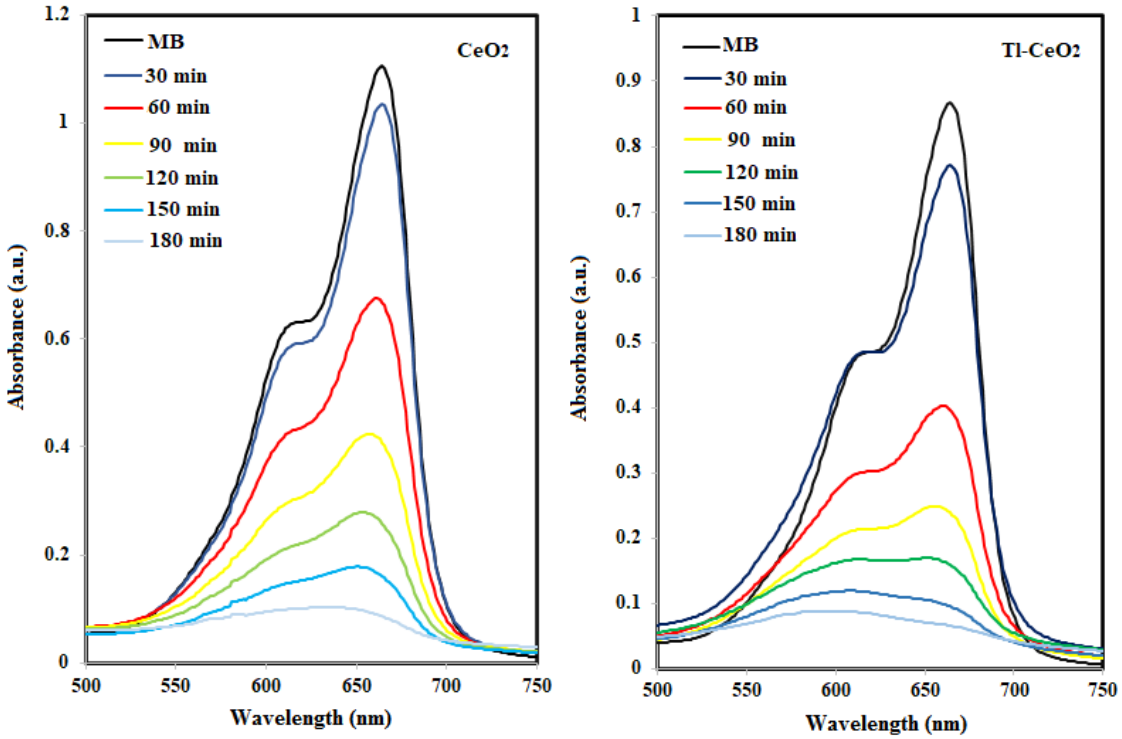

Fig. 7. Degradation of aqueous MB dye by pure and Tl-CeO2-NP photocatalysis under UVA light.

concentrations (1–1000 µg/mL) of synthesized nanoparticles through the application of MTT assay for 24 h (Fig. 6). The cytotoxic outcomes of the NP on the cancer cells (MDA-MB-231) are depicted in Fig. 6, which lacked the presence of any significant cytotoxicity effect even at the concentration of 400 µg/mL. Therefore, it can be concluded that cytotoxic effects of metals, such as Tl, can be greatly reduced through the doping process, which would provide their application for medical and industrial purposes with a guaranteed safety.

Photocatalytic activity

We studied the photocatalytic performance of pure and Tl-CeO_2-NP against MB dye degradation sub UV-light and the obtained outcomes are presented in Fig. 7. Accordingly, the degradation rates of MB dye were estimated to be about 88.75 and 93.11% after its exposure to pure and Tl-CeO_2-NPs for 180 min, respectively. The best photocatalyst activity was explicitly observed from the case of Tl-CeO_2-NP, which was in correspondence with the UV-Vis outcomes. It is therefore indicated that the distribution of Tl-CeO_2-NP can be an effective approach for placing more active sites on the surface of photocatalyst. Based on the band-gap and FESM outcomes, Tl-CeO_2-NP contained a lower band-gap and smaller particle size, which resulted in a faster electron transferring between the valence band and conduction band of thallium and increased the excited electrons of CeO_2, leading to a higher degradation rate of methylene blue.

CONCLUSION

The synthesis of pure and Tl-CeO_2-NP were successfully conducted through the *Prosopis fracta* extract, and the physicochemical properties of our products were determined by using identification devices such as PXRD, UV-Vis, and FESEM. The obtained data confirmed the uniformed and porous structure of nanoparticles at the range of nanoscale. The process of doping with different metals resulted in inducing alterations in the particle size. According to the photocatalytic performance of NPs, Tl-CeO_2-NP exhibited a superior degradation against MB dye due to its smaller particle size and lower band-gap. Furthermore, we surveyed the toxic functionality of synthesized NPs on MDA-MB-231 cell lines by the MTT test and the outcomes displayed the non-toxic effects of pure and doped CeO_2-NP. Based on these finding, we can confirm the applicability of our NP for biological

applications and cancer treatment, as well as suggest this product as a potential and cost-effective option for the degradation of environmental pollutants.

CONFLICT OF INTEREST

The authors declare no conflict of interest.

REFERENCES

1. Baig, N., I. Kammakakam, and W. Falath, Nanomaterials: A review of synthesis methods, properties, recent progress, and challenges. Materials Advances, 2021. 2(6): p. 1821-1871. https://doi.org/10.1039/D0MA00807A
2. Sarani, M., et al., Study of in vitro cytotoxic performance of biosynthesized α-Bi2O3 NPs, Mn-doped and Zn-doped Bi2O3 NPs against MCF-7 and HUVEC cell lines. Journal of Materials Research and Technology, 2022. 19: p. 140-150. https://doi.org/10.1016/j.jmrt.2022.05.002
3. Behzad, F., et al., An overview of the plant-mediated green synthesis of noble metal nanoparticles for antibacterial applications. Journal of Industrial and Engineering Chemistry, 2021. 94: p. 92-104. https://doi.org/10.1016/j.jiec.2020.12.005
4. Ahmed, M., S.T. Bishay, and M.M. El-Masry, Structural and topographic study of ceria nanoparticles prepared via different techniques. Superlattices and Microstructures, 2015. 77: p. 240-255. https://doi.org/10.1016/j.spmi.2014.10.023
5. Khan, M., et al., Efficacy of Green Cerium Oxide Nanoparticles for Potential Therapeutic Applications: Circumstantial Insight on Mechanistic Aspects. Nanomaterials, 2022. 12(12): p. 2117. https://doi.org/10.3390/nano12122117
6. Sun, C., H. Li, and L. Chen, Nanostructured ceria-based materials: synthesis, properties, and applications. Energy & Environmental Science, 2012. 5(9): p. 8475-8505. https://doi.org/10.1039/c2ee22310d
7. Muddather, H.F., M.M. Elhassan, and A. Faggad, Survival outcomes of breast cancer in sudanese women: a hospital-based study. JCO Global Oncology, 2021. 7(1): p. 324-332. https://doi.org/10.1200/GO.20.00538
8. Mosleh-Shirazi, S., et al., Biosynthesis, simulation, and characterization of Ag/AgFeO2 core-shell nanocomposites for antimicrobial applications. Applied Physics A, 2021. 127(11): p. 1-8. https://doi.org/10.1007/s00339-021-05005-7
9. Riehemann, K., et al., Nanomedicine-challenge and perspectives. Angewandte Chemie International Edition, 2009. 48(5): p. 872-897. https://doi.org/10.1002/anie.200802585
10. Miri, A., S. Akbarpour Birjandi, and M. Sarani, Survey of cytotoxic and UV protection effects of biosynthesized cerium oxide nanoparticles. Journal of Biochemical and Molecular Toxicology, 2020. 34(6): p. e22475. https://doi.org/10.1002/jbt.22475
11. Miri, A., et al., Cerium oxide nanoparticles: green synthesis using Banana peel, cytotoxic effect, UV protection and their photocatalytic activity. Bioprocess and Biosystems Engineering, 2021. 44(9): p. 1891-1899. https://doi.org/10.1007/s00449-021-02569-9
12. Maleki, P., et al., Green facile synthesis of silver-doped cerium oxide nanoparticles and investigation of their cytotoxicity and antibacterial activity. Inorganic Chemistry Communications, 2021. 131: p. 108762. https://doi.org/10.1016/j.inoche.2021.108762
13. Mondal, P., S. Baksi, and D. Bose, Study of environmental issues in textile industries and recent wastewater treatment technology. World Scientific News, 2017. 61(2): p. 94-105.
14. Lellis, B., et al., Effects of textile dyes on health and the environment and bioremediation potential of living organisms. Biotechnology Research and Innovation, 2019. 3(2): p. 275-290. https://doi.org/10.1016/j.biori.2019.09.001
15. Dutta, S., et al., Recent advances on the removal of dyes from wastewater using various adsorbents: A critical review. Materials Advances, 2021. https://doi.org/10.1039/D1MA00354B
16. Aziz, F., et al., A review on synergistic coexisting pollutants for efficient photocatalytic reaction in wastewater remediation. Environmental Research, 2022. 209: p. 112748. https://doi.org/10.1016/j.envres.2022.112748
17. Liu, H., C. Wang, and G. Wang, Photocatalytic advanced oxidation processes for water treatment: recent advances and perspective. Chemistry-An Asian Journal, 2020. 15(20): p. 3239-3253. https://doi.org/10.1002/asia.202000895
18. Khan, M.M., et al., Modifications in structural, morphological, optical and photocatalytic properties of ZnO: Mn nanoparticles by sol-gel protocol. Materials Science in Semiconductor Processing, 2018. 87: p. 134-141. https://doi.org/10.1016/j.mssp.2018.07.016
19. Gómez, D.A., J. Coello, and S. Maspoch, The influence of particle size on the intensity and reproducibility of Raman spectra of compacted samples. Vibrational spectroscopy, 2019. 100: p. 48-56. https://doi.org/10.1016/j.vibspec.2018.10.011
20. Hamidian, K., et al., Photocatalytic performance on degradation of Acid Orange 7 dye using biosynthesized un-doped and Co doped CeO2 nanoparticles. Materials Research Bulletin, 2021. 138: p. 111206. https://doi.org/10.1016/j.materresbull.2021.111206